Materials Today Bio 31 (2025) 101449

Contents lists available at ScienceDirect

Materials Today Bio

journal homepage: www.journals.elsevier.com/materials-today-bio

# A bioprinted animal patient-derived breast cancer model for anti-cancer drug screening

Xuan Mei [a], Maria Fernanda Uribe Estrada [a], Muhammad Rizwan [a,b], Izeia Lukin [a,c,d], Begoña Sanchez Gonzalez [a], Jose Gerardo Marin Canchola [a], Valeria Velarde Jarquín [a], Ximena Salazar Parraguez [a], Francisco Del Valle Rodríguez [a], Carlos Ezio Garciamendez-Mijares [a], Zeng Lin [a], Jie Guo [a], Zhenwu Wang [a], Sushila Maharjan [a], Gorka Orive [c,d,e,f,g], Yu Shrike Zhang [a,*]

[a] Division of Engineering in Medicine, Department of Medicine, Brigham and Women's Hospital, Harvard Medical School, Cambridge 02139, MA, USA
[b] Cancer Genetics & Epigenetics Research Group, Department of Biosciences, COMSATS University Islamabad, Park Road Islamabad 45550, Pakistan
[c] NanoBioCel Research Group, School of Pharmacy, University of the Basque Country (UPV/EHU), Vitoria-Gasteiz 01006, Spain
[d] Bioaraba, NanoBioCel Research Group, Vitoria-Gasteiz 01009, Spain
[e] Biomedical Research Networking Centre in Bioengineering, Biomaterials and Nanomedicine (CIBER-BBN), Vitoria-Gasteiz, Spain
[f] University Institute for Regenerative Medicine and Oral Implantology - UIRMI (UPV/EHU-Fundación Eduardo Anitua), Vitoria-Gasteiz, 01007, Spain
[g] Singapore Eye Research Institute, Singapore 169856, Singapore

A B S T R A C T

Animal models are commonly used for drug screening before clinical trials. However, developing these models is time-consuming, and the results obtained from these models may differ from clinical outcomes due to the differences between animals and humans. To this end, 3D bioprinting offers several advantages for drug screening, such as high reproducibility and improved throughput, in addition to the human cells that can be used to generate these models. Here, we report the development of an animal patient-derived *in vitro* breast cancer model for drug screening using digital light processing (DLP) bioprinting. These bioprinted models demonstrated good cytocompatibility and preserved phenotypes of the cells. DLP enabled rapid fabrication with blood vessel-like channels to replicate, to a good extent, the tumor microenvironment. Our findings suggested that the improved microenvironment, provided by vascular structures within the bioprinted models, played a crucial role in reducing the chemoresistance of drugs. In addition, the correlation of the *in vitro* and *in vivo* drug-screening results was preliminarily performed to evaluate the predictive feasibility of this bioprinted model, suggesting a potential strategy for the design of future drug-testing platforms.

## 1. Introduction

Due to the complexity of internal organs, animal models have long been essential in drug testing [1,2], providing critical data on drug safety, efficacy, and potential side effects before progressing to human trials [3,4]. However, these models come with limitations, including high costs, long timelines, biological variability, and ethical concerns [5], which can make them difficult to predict how a drug will perform across diverse populations, for example [6]. Additionally, the differences between animal and human physiology sometimes lead to unreliable results [7]. Recognizing these challenges, the United States Food and Drug Administration (FDA) has recently reemphasized that certain new drugs may no longer require traditional animal tests [8], reflecting an effort to streamline drug-approval processes while maintaining safety. In response, researchers have been exploring alternative methods to provide more accurate and ethical platforms for drug testing, such as 3D cell cultures [9,10].

While 2D cultures fail to replicate the complex 3D architectures of tissues [11,12], 3D models provide more realistic microenvironments, allowing for better cell-cell and cell-matrix interactions [13,14]. However, conventional 3D culture methods, such as organoids and spheroids, typically involve combining cells in a relatively simple or uncontrolled manner without adequately mimicking the intricate structures and functions of actual organs [15]. To address this limitation, new technologies such as 3D bioprinting have been extensively studied for their abilities to create more precise tissue models [16,17]. Unlike organoids and spheroids, which rely on the self-organization of cells, bioprinting enables precise control over the spatial arrangements

This article is part of a special issue entitled: Light-based 3D bioprinting applications published in Materials Today Bio.

* Corresponding author.
*E-mail address:* yszhang@bwh.harvard.edu (Y.S. Zhang).

https://doi.org/10.1016/j.mtbio.2025.101449
Received 16 September 2024; Received in revised form 23 November 2024; Accepted 3 January 2025
Available online 3 January 2025

of cells, allowing the creation of intricate tissue architectures [18]. While organoids and spheroids often suffer from batch-to-batch variability [19], bioprinted models, in contrast, offer consistency in production, making them favorable for reproducible higher-throughput drug screening [20]. Among these technologies, extrusion and digital light processing (DLP)-based bioprinting methods have gained significant attentions [21–23]. DLP, in particular, stands out for its high resolution and speed, which enable the fabrication of detailed, biomimetic structures [24,25]. Different from extrusion-based bioprinting, which plots materials to form constructs in a point-by-point manner, DLP uses light to solidify bioinks directly layer-by-layer, resulting in smoother, more accurate models in many scenarios [26,27]. With its high speed, and resolution down to tens of micrometers when producing volumetric patterns [28], DLP holds great promise in drug screening, where the accurate replication of tissue structures is crucial for predicting how drugs would interact with real human organs [29,30].

In this work, we developed a 3D-bioprinted breast cancer model platform that may contribute to personalizable anti-breast-cancer drug screening. We first constructed an *in vivo* mouse tumor model, and then extracted the animal patient-derived tumor cells to build the *in vitro* models, hoping to replicate the original tumor characteristics to improve the precise of drug screening results. Gelatin methacryloyl (GelMA) was used for the preparation of bioink to preserve cell viability and phenotype. The *in vitro* models were built through DLP bioprinting, where blood vessel-like channels were produced to simulate physiological vascular structures. To evaluate the platform, we tested the responses of the bioprinted tumor models to two FDA-approved anti-cancer drugs, doxorubicin (DOX) and capecitabine (CAP). In addition, the *in vitro* drug-screening results collected from the bioprinted models were preliminarily cross-validated with the corresponding *in vivo* results from

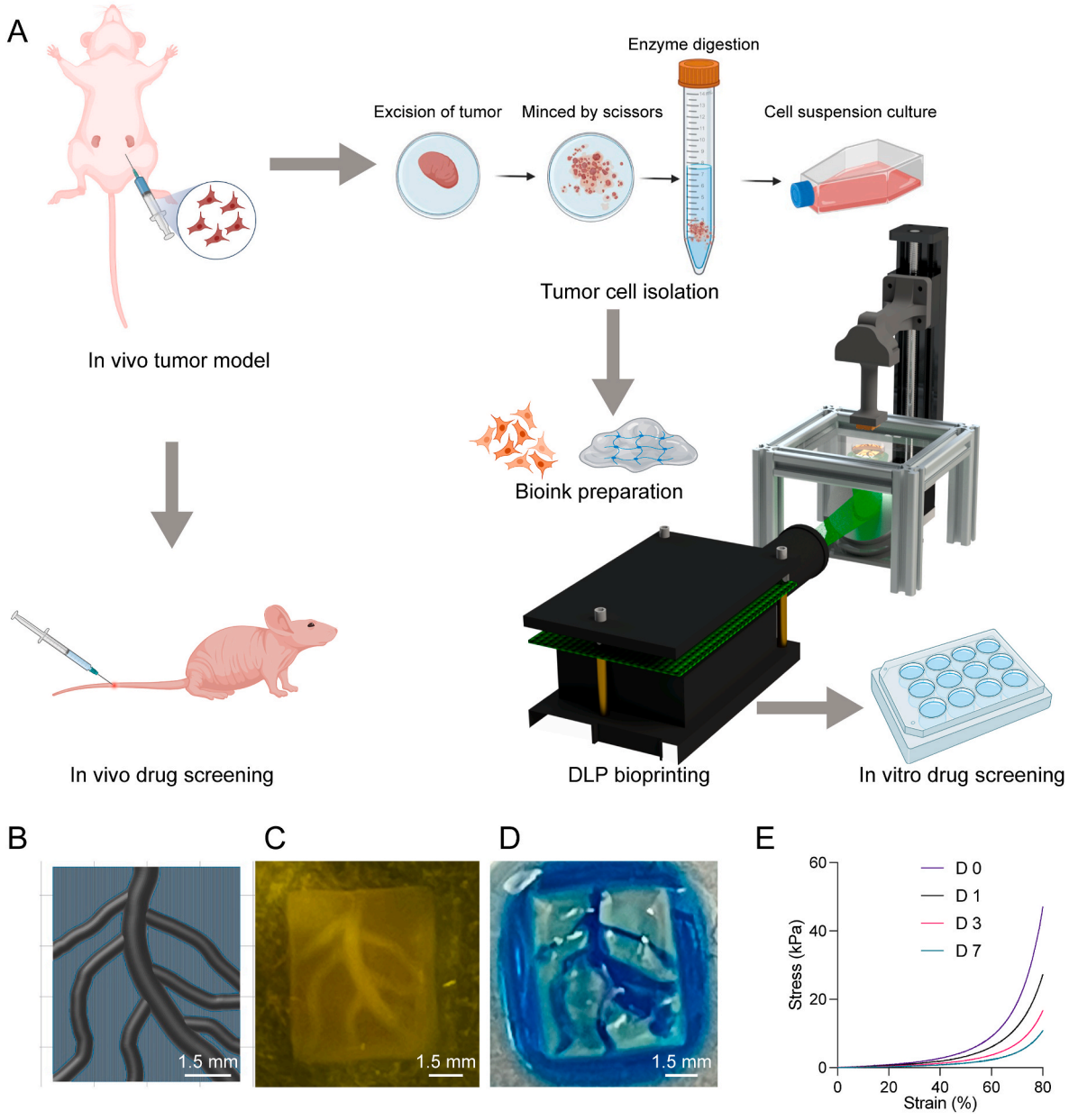


**Fig. 1. Fabrication and characterizations of the bioprinted constructs. (A)** Schematic showing the workflow including *in vivo* tumor model-building, breast cancer model-bioprinting, as well as *in vitro* and *in vivo* drug screening. **(B)** CAD designs of the bioprinted tumor model with blood vessel-like channels. **(C)** Photograph of the bioprinted breast cancer model with the channels. The size of the model was 7.5 × 5.5 × 2.5 (L × W × H) $mm^3$. **(D)** Perfusion with a blue dye to show the connectivity of the bioprinted channels. **(E)** The compressive stress-strain curves of the bioprinted constructs immersed within the culture medium for different days. (For interpretation of the references to colour in this figure legend, the reader is referred to the Web version of this article.)

mice. The development of this platform enables the recreation of an individual patient's tumor microenvironment, including blood vessel-like channels, which may improve the accuracy of predicting drug effects in the body for patient-specific anti-cancer drug screening in the future with further optimizations.

## 2. Results and discussion

### 2.1. Fabrication of in vitro breast cancer models with blood vessel-like structures using DLP bioprinting

Fig. 1A illustrates the comprehensive workflow adopted in this

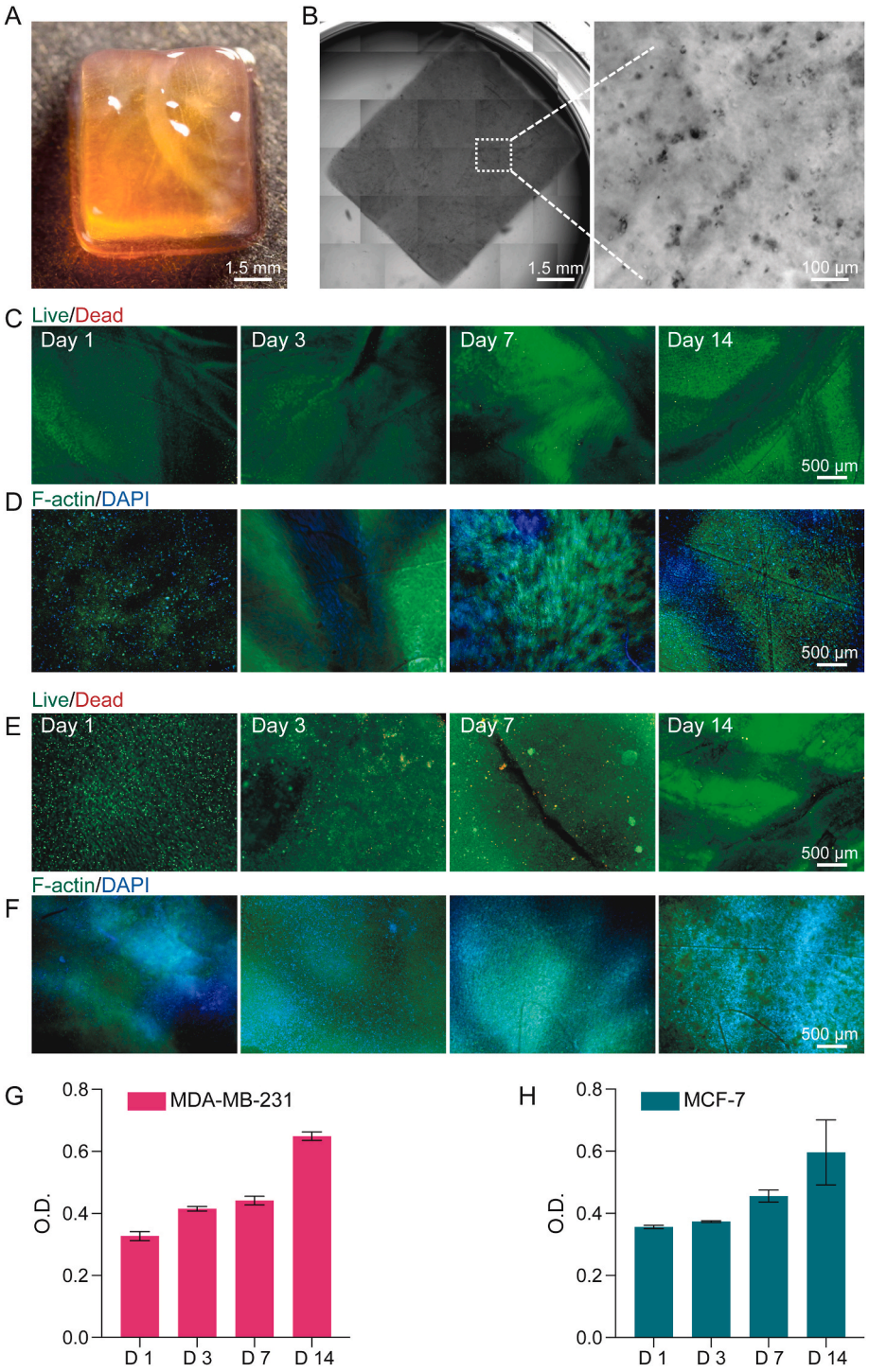


**Fig. 2. Cell viability and proliferation within bioprinted breast tumor models. (A)** Photograph of the bioprinted tumor model incorporating MDA-MB-231 cells isolated from the mouse tumor. **(B)** Optical micrographs showing cells within the bioprinted constructs. Right panel shows the enlarged image from the selected area in the left image. **(C)** and **(E)** Live/dead staining of (C) MDA-MB-231 and (E) MCF-7 cells at 1, 3, 7, and 14 days of culture, where live cells were stained with green fluorescence and dead cells with red fluorescence. **(D)** and **(F)** F-acting (green) staining for (D) MDA-MB-231 and (F) MCF-7 cells at 1, 3, 7, and 14 days of culture. Nuclei of cells were stained with 4′,6-diamidino-2-phenylindole (DAPI) (blue). **(G)** and **(H)** MTS assay performed on (G) MDA-MB-231 and (H) MCF-7 cells cultured for 1, 3, 7, and 14 days. n = 4, mean ± SD. (For interpretation of the references to colour in this figure legend, the reader is referred to the Web version of this article.)

study. Starting from the creation of the *in vivo* tumor model in mice, breast cancer cells were isolated to formulate the bioink for bioprinting the *in vitro* models and subsequent drug screening. In the meanwhile, *in vivo* drug screening was performed in parallel as a comparison. The computer-aided design (CAD) in Fig. 1B depicts the blood vessel-like structure embed in the bioprinted tumor model. DLP was employed to bioprint the constructs with the channels being visible (Fig. 1C), demonstrating the capability of the bioprinting process to create channel-laden structures that are crucial for replicating the tumor physiology potentially. To show the perfusion capability of the bioprinted channel, a blue dye was injected from one end of the channel. The successful perfusion of the bioprinted vascular pattern was observed (Fig. 1D), indicating the patency and connectivity of the channels. Such perfusion also revealed that the bioprinted vascular structures were functional and capable of fluid-transport, which is essential for mimicking the nutrient and waste-exchanges in living tissues [31].

To evaluate the printing fidelity, the angles of the printed constructs were measured and compared to those from the CAD model (Fig. S1A). Printing fidelity was quantified as the ratio of the printed construct measurements relative to the CAD model, with a ratio of 100 % indicating no deviation. As shown in Fig. S1B, all the six measured angles revealed ratios close to 100 %, demonstrating high printability and fidelity. Since the bioprinted structures were planned to be further used for longer-term cell culture, we tracked the mechanical property-change of the bioprinted constructs for 7 days in cell culture medium. As shown in Fig. 1E, the compressive stress-strain curves suggested that the stiffness of GelMA decreased along with the culture time, which may facilitate the bioprinting process for structural construction in the beginning and support the cell growth afterwards.

### 2.2. Cell survival and proliferation within bioprinted breast tumor models

As we have demonstrated the bioprinting of constructs with channels, tumor cells isolated from the mouse tumor tissues were further utilized to bioprint the breast cancer models for drug screening. The mouse tumor models were built first, and the tumors were harvested after reaching a certain size (Figs. S2A and S2B). To isolate the cells for bioprinting, the tumors were excised, minced, and digested with enzymes. Fig. 2A shows the bioprinted tumor model incorporating MDA-MB-231 cells isolated from mouse tumors. The vascular channels were still clearly visible. From the enlarged optical micrographs, the cells were dispersed uniformly after bioprinting (Fig. 2B). To investigate the cell viability within the bioprinted constructs, live/dead staining of cells was conducted at different time points. The green fluorescence indicates live cells, while the red fluorescence indicates dead cells. Fig. 2C shows live/dead staining results of MDA-MB-231 cells over time within the bioprinted models. Only a few dead cells (red) were observed, demonstrating the suitability of the bioprinted environment for cell survival. Fig. 2D displays MDA-MB-231 cells stained for F-actin (green) and nuclei (blue) at 1, 3, 7, and 14 days of culture. The consistent staining patterns indicated maintained cellular structure and integrity over the culture period that we evaluated. Cell metabolic activities were measured using 3-(4,5-dimethylthiazol-2-yl)-5-(3-carboxymethoxyphenyl)-2-(4-sulfophenyl)-2H-tetrazolium (MTS) assay for 14 days. The data showed an increase in metabolic activity over time (Fig. 2G), suggesting that the cells were proliferating within the bioprinted constructs.

Similar results were observed with MCF-7 cell-laden bioprinted model. The live/dead staining indicated that robust cell survival was present (Fig. 2E). MCF-7 cells were growing well with good proliferation behaviors within bioprinted constructs for 14 days as indicated by F-actin staining (Fig. 2F) and MTS assay (Fig. 2H). As a comparison, the proliferation of 2D-cultured cells in well plates was assessed (Fig. S3). Unlike the 3D-bioprinted models, both MDA-MB-231 and MCF-7 cells showed decreased proliferation from Day 7 to Day 14, likely due to the limited available areas in well plates.

### 2.3. Characterizations of mouse tumor cells within bioprinted models

After confirming the viability and proliferation of the cells after bioprinting, immunostaining was performed to characterize the mouse tumor-isolated cells within the bioprinted models. As shown in Fig. 3A and B, the MDA-MB-231 cells exhibited poor cell-cell adhesion and lacked expression of E-cadherin, which is a characteristic epithelial marker [32]. In contrast, the MCF-7 cells expressed E-cadherin, consistent with their features as differentiated mammary epithelial cells [33]. The staining results also demonstrated that the MDA-MB-231 cells remained dual-positive for CK8 and CK5, while the MCF-7 cells were CK8-positive and CK5-negative, which is in consistency with the characteristics of reported protein-expressions for both cells [34]. These findings confirmed that the bioprinting process did not alter the phenotypic characteristics of the tumor cells, preserving the tumor microenvironments *in vitro* when isolated from the animal tumors.

In addition, immunofluorescence staining was performed on MDA-MB-231 cells for Ki67, which is recognized as a proliferation marker for cancer cells [35]. A significant proportion of cells within the bioprinted constructs showed green signals in the nuclei (stained with DAPI) (Fig. 3C), confirming the proliferation of cells and the active growth of the tumor model. Ki67 was detected in MCF-7 cells as well (Fig. 3D), implying that the cells were proliferative. The above results proved that we successfully constructed the *in vitro* breast cancer models with two different breast cancer cell types derived from respective animal tumors, which maintained specific cancer cell markers and could be potentially used for drug screening.

### 2.4. In vitro drug-screening studies

The *in vitro* drug screening was conducted in a well plate (Fig. S4), which focused on evaluating the responses of bioprinted breast cancer models to two commonly used anti-cancer drugs: DOX and CAP. The effectiveness of these drugs was assessed by calculating the half-maximal inhibitory concentration ($IC_{50}$) values, which represents the concentration required to inhibit cell viability by 50 % [36]. The bioprinted breast cancer models were subjected to different dosages of DOX and CAP for $IC_{50}$ calculations. As the control, constructs without the channels were also fabricated to evaluate the drug responses. For the MDA-MB-231 cell-laden model, $IC_{50}$ values of DOX were calculated as 253.4 μg $mL^{-1}$ for the constructs with channels and 1171 μg $mL^{-1}$ for the ones without channels (Fig. 4A). The $IC_{50}$ values of CAP were calculated as 218.8 μg $mL^{-1}$ for the constructs with channels and 859.7 μg $mL^{-1}$ for the ones without channels (Fig. 4B). As for MCF-7 cell-based model, $IC_{50}$ values of DOX were calculated as 177.5 μg $mL^{-1}$ for the constructs with channels and 208.6 μg $mL^{-1}$ for the ones without channels (Fig. 4C). The $IC_{50}$ values of CAP were calculated as 806.0 μg $mL^{-1}$ for the constructs with channels and 1925 μg $mL^{-1}$ for the ones without channels (Fig. 4D).

The lower $IC_{50}$ values in constructs with channels suggested that these models had less chemoresistance than those without channels to both DOX and CAP [37]. These results supported that the inclusion of channels would more closely mimic the physiological conditions, such as nutrient-transport and waste-removal, which are critical components of the tumor microenvironment. This improved modeling of *in vivo* conditions likely could allow for more realistic drug diffusion and cellular interactions, thereby making the cells more sensitive to the drugs in the constructs with channels compared to those without.

### 2.5. In vivo drug screening studies and preliminary in vitro-in vivo correlations

To explore the potential relevance of drug effects on the bioprinted *in vitro* tumor models to the *in vivo* model, different dosages (1 mg $mL^{-1}$ and 0.5 mg $mL^{-1}$) of DOX and CAP were also tested on mice carrying the respective tumors through intravenous injection. These dosage-

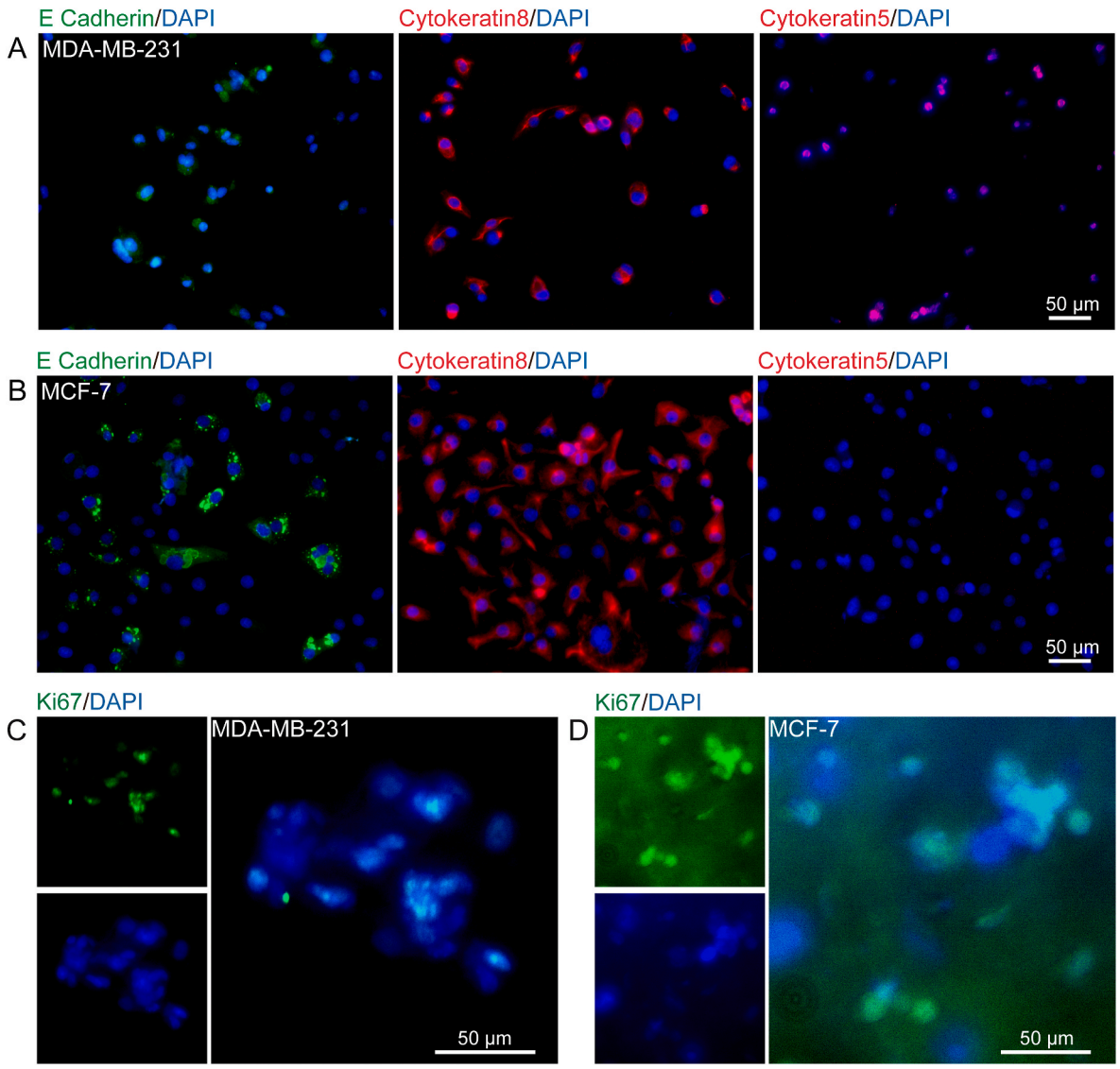


**Fig. 3. Characterizations of mouse tumor cells within the bioprinted models. (A)** and **(B)** Immunostaining characterizations of mouse tumor-isolated (A) MDA-MB-231 and (B) MCF-7 cells within the bioprinted constructs. The cells were stained for E-cadherin (green), cytokeratin 5 (CK5) or cytokeratin 8 (CK8) (red), and nuclei (blue). **(C)** and **(D)** Fluorescence micrographs of mouse tumor-isolated (C) MDA-MB-231 cells and (D) with Ki67 (green) immunostaining and DAPI staining for nuclei (blue) at day 14. (For interpretation of the references to colour in this figure legend, the reader is referred to the Web version of this article.)

selections align with pharmacological profiles from previous animal studies, ensuring translational relevance while managing side effects effectively [38,39]. For DOX, 0.5 mg $mL^{-1}$ was chosen as it is a well-established dose that has been shown to effectively suppress tumor growth while minimizing cardiotoxicity. Similarly, for CAP, both 0.5 mg $mL^{-1}$ and 1 mg $mL^{-1}$ of doses were used to explore the dose-response relationship. The dose at 0.5 mg $mL^{-1}$ served as a lower effective value with reduced toxicity, whereas the dose at 1 mg $mL^{-1}$ allowed assessment of the potential for enhanced efficacy at a higher concentration.

Fig. 5A presents tumor volume measurements after treatments with different dosages of drugs on mice. For the control groups without injection of drugs, the tumor volumes remained increasing within 7 days. The tumor volumes of drug-treated groups decreased along with the culture time. Specifically, the dosages here for the *in vivo* studies were 1 mg $mL^{-1}$ and 0.5 mg $mL^{-1}$, which were 30 mg $m^{-2}$ and 15 mg $m^{-2}$, respectively, when normalized to body surface area (BSA)-based dosages [40].

As a comparison, the $IC_{50}$ values calculated from our *in vitro* bioprinted models were 908.2 mg $m^{-2}$ for DOX on MDA-MB-231, 784.2 mg $m^{-2}$ for CAP on MDA-MB-231, 636.2 mg $m^{-2}$ for DOX on MCF-7, and 2888 mg $m^{-2}$ for CAP on MCF-7. The comparison between *in vitro* (bioprinted models) and *in vivo* (mouse models) responses to DOX and CAP revealed significantly higher $IC_{50}$ values in the bioprinted models. For MDA-MB-231 cells, the $IC_{50}$ for DOX was 30.3 times higher than the *in vivo* dosage, and for CAP it was 26.1 times higher. For DOX on MCF-7 cells, the $IC_{50}$ was 21.2 times higher than the *in vivo* dosage, while for CAP it was 96.3 times higher, suggesting substantial resistance to CAP in particular. A higher $IC_{50}$ indicates reduced drug efficacy, meaning a higher dosage is required to inhibit cancer cell growth. In the *in vivo* models, a lower dosage effectively reduced tumor size, while the higher dosage required in the *in vitro* models suggested that differences still remained between the two systems, which likely arose from factors such as the absence of *in vivo* metabolic clearance in the 3D-bioprinted structures, and variations in microenvironmental conditions. This resistance observed in the bioprinted models may mimic a more challenging tumor microenvironment, which could be advantageous for testing higher drug doses or combination therapies but also underscores the complexities in translating *in vitro* models to *in vivo* applications.

Fig. 5B further shows H&E staining of tumor sections from mice after treatment, where hematoxylin stains cell nuclei purplish blue and eosin

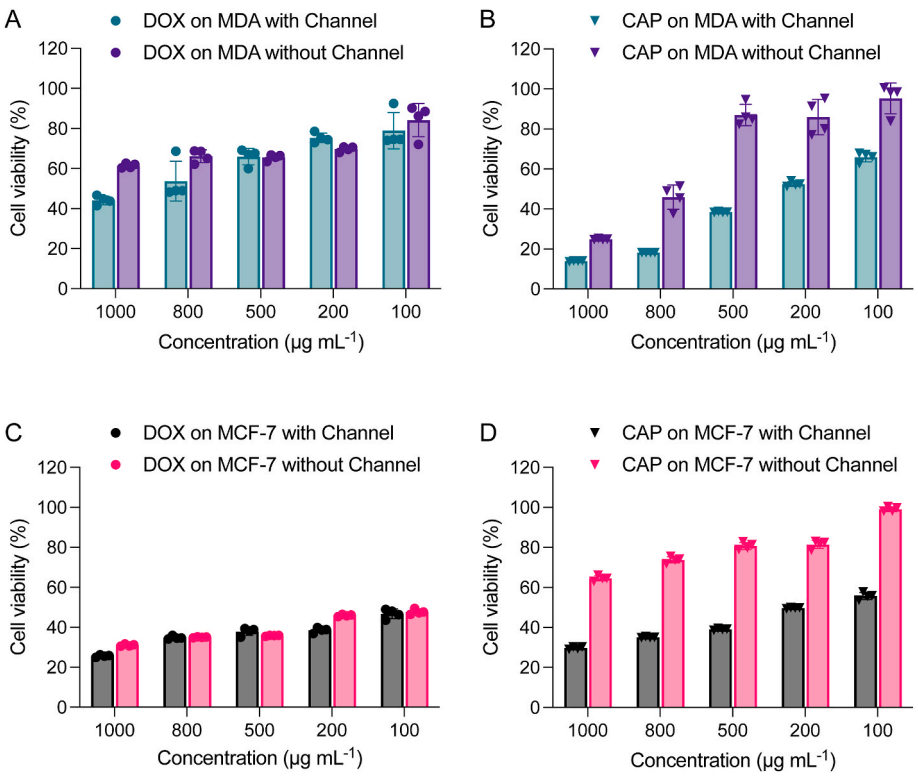


**Fig. 4. Comparisons of the sensitivities of the bioprinted breast cancer models to different anticancer drugs. (A)** and **(B)** Cell viability evaluations of MDA-MB-231 cells within bioprinted models with or without channels in responses to (A) DOX and (B) CAP. **(C)** and **(D)** Cell viability evaluations of MCF-7 cells within bioprinted models with or without channels in responses to (C) DOX and (D) CAP. n = 4, mean ± SD.

stains the cytoplasm and extracellular matrix pink [41]. Significant areas of necrosis were observed from the tumor sections, with tumor cells displaying characteristic nuclear fragmentation, contraction, and dissolution. The stained sections provided further histological evidence of the drug effects on the tumor tissues, comparing to the tumor volume changes.

## 3. Conclusions

In this work, we built *in vitro* breast cancer models through DLP bioprinting, which were further used for drug screening. The cancer cells used for bioprinting were collected from mice and the correlation of *in vitro* and *in vivo* drug screening results were analyzed. We utilized GelMA to produce the bioink for bioprinting, as it offers good cytocompatibility, which is an essential requirement for constructing a drug screening system. As confirmed by immunostaining, these bioprinted models allowed the cells to survive for up to 14 days that we tested, while also sufficiently retaining their phenotypes. In terms of the methodology, DLP provides benefits in bioprinting samples in large quantities and repeatably. The speed and repeatability of fabrication are crucial to further support higher-throughput drug screening, which also becomes a prerequisite for relevant preclinical applications [42,43]. Another advantage brought by DLP is the ability in constructing fine structures [44], for example blood vessel-like patterns shown in this work. The improvement is not only the more realistic biological structure, but also the better function.

The presence of these channels was associated with decreased chemoresistance, which was reflected on the drug screening results. Cancer models with blood vessel-like channels exhibited more sensitivities to both DOX and CAP comparing to those without channels (Fig. 4). However, even with the channels, the dosages calculated from our bioprinted models were significantly higher than those from *in vivo* (Fig. 5). In addition, when comparing the *in vitro* $IC_{50}$ values from those of bioprinted models to clinical dosages, that is 40–75 mg $m^{-2}$ (intravenous) for DOX [45,46] and 2500 mg $m^{-2}$ (oral) for CAP [47], the $IC_{50}$ for DOX in MDA-MB-231 cells (908.2 mg $m^{-2}$) was much higher than the clinical range. Interestingly, the $IC_{50}$ for CAP (2888 mg $m^{-2}$) was similar to the clinical oral dosage. This observation suggested that while the bioprinted model may not fully replicate conditions for intravenous injections, it may more closely mimic the tumor microenvironment that is favorable for oral drug administration. Overall, the discrepancy between the higher $IC_{50}$ values in the bioprinted models and the clinical dosages underscores the challenges of replicating the *in vivo* tumor microenvironment *in vitro*, which may result in differences in cell-to-cell interactions, nutrient gradients, and drug metabolism [48–50]. Here, the bioprinted models with channels partially simulated critical aspects of the tumor microenvironment, while constructs without channels showed even higher $IC_{50}$ values, emphasizing that more simplified models lacking these microenvironmental features would be less representative of the *in vivo* conditions.

The current study, while demonstrating the potential of 3D-bioprinted breast cancer models for drug screening, has several limitations that should be considered. One primary limitation is the challenge to fully replicate the complexity of the *in vivo* tumor microenvironments. Although the integration of vascular-like channels in the bioprinted models may improve nutrient and drug perfusion, it cannot fully mimic the dynamic interactions between tumor cells, immune cells, and other components in the presented configurations. Another limitation is the observed discrepancy between the drug sensitivities of the *in vitro* and *in vivo* models, as indicated by the higher $IC_{50}$ values in the bioprinted constructs compared to *in vivo* results. This difference likely resulted from factors such as the lack of metabolic clearance mechanisms in the bioprinted models, which are present in living organisms, and differences in drug distribution and diffusion between the two systems. Additionally, the study focuses on a limited number of drug compounds, specifically DOX and CAP, which may not entirely represent the

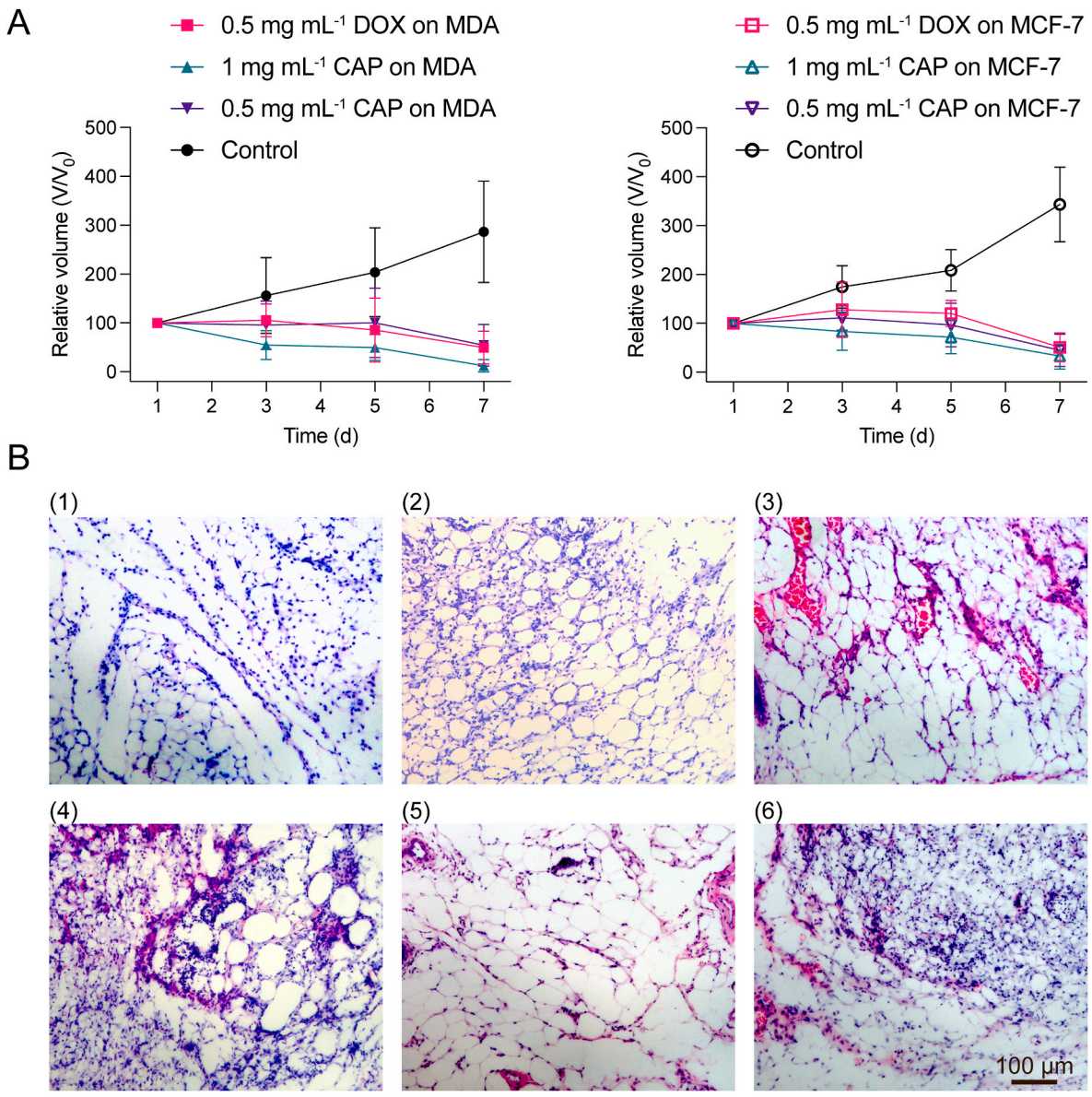


**Fig. 5.** ***In vivo*** **drug screening on animal models. (A)** Tumor volume-changes of mice bearing the MDA-MB-231 or MCF-7 tumor. Mice were treated with DOX (0.5 mg $mL^{-1}$) and CAP (0.5 mg $mL^{-1}$ and 1 mg $mL^{-1}$) separately. n = 4, mean ± SD. **(B)** Hematoxylin and eosin (H&E) staining of the sections collected from the mouse tumors. The groups are listed as below: Mice bearing MDA-MB-231 tumor treated with (1) 0.5 mg $mL^{-1}$ DOX, (2) 0.5 mg $mL^{-1}$ CAP and (3) 1 mg $mL^{-1}$ CAP; mice bearing MCF-7 tumor treated with (4) 0.5 mg $mL^{-1}$ DOX, (5) 0.5 mg $mL^{-1}$ CAP and (6) 1 mg $mL^{-1}$ CAP.

diversity of therapeutic agents used in clinical settings. Expanding the range of drugs tested could provide a more comprehensive evaluation of the models' predictive capabilities. Furthermore, despite that the study suggested that the bioprinted models could potentially serve as a platform for patient-specific drug testing, further validation with a larger number of patient-derived samples would be needed to confirm their predictive accuracies and applicability. Addressing these shortcomings in future studies will enhance the models' utilities in preclinical drug screening and personalized medicine. Together, our results, although still preliminary, highlighted the importance of modeling the tumor microenvironment accurately to improve the predictive value of drug responses, pointing to the need for continued refinement of these models to better-match clinical outcomes in the future.

## CRediT authorship contribution statement

**Xuan Mei:** Writing – review & editing, Writing – original draft, Visualization, Validation, Methodology, Investigation, Formal analysis, Data curation. **Maria Fernanda Uribe Estrada:** Writing – review & editing, Investigation, Formal analysis, Data curation. **Muhammad Rizwan:** Writing – review & editing, Investigation, Formal analysis, Data curation. **Izeia Lukin:** Writing – review & editing, Investigation, Data curation. **Begoña Sanchez Gonzalez:** Writing – review & editing, Investigation, Data curation. **Jose Gerardo Marin Canchola:** Writing – review & editing, Investigation, Data curation. **Valeria Velarde Jarquín:** Writing – review & editing, Investigation, Data curation. **Ximena Salazar Parraguez:** Writing – review & editing, Investigation, Data curation. **Francisco Del Valle Rodríguez:** Writing – review & editing, Data curation. **Carlos Ezio Garciamendez-Mijares:** Writing – review & editing, Software. **Zeng Lin:** Writing – review & editing, Data curation. **Jie Guo:** Writing – review & editing, Data curation. **Zhenwu Wang:** Writing – review & editing, Methodology. **Sushila Maharjan:** Writing – review & editing, Methodology. **Gorka Orive:** Writing – review & editing, Methodology. **Yu Shrike Zhang:** Writing – review & editing, Writing – original draft, Resources, Project administration, Methodology, Funding acquisition, Conceptualization.

## Declaration of Competing Interest

The authors declare the following financial interests/personal relationships which may be considered as potential competing interests: Yu Shrike Zhang reports financial support was provided by National Institutes of Health. Yu Shrike Zhang reports financial support was provided by National Science Foundation. Yu Shrike Zhang reports financial support was provided by Brigham and Women's Hospital Biomedical Research Institute. Yu Shrike Zhang reports a relationship with Xellar Biosystems that includes: board membership, consulting or advisory, and equity or stocks. If there are other authors, they declare that they have no known competing financial interests or personal relationships that could have appeared to influence the work reported in this paper.

## Acknowledgement

The work is supported by the National Institutes of Health (R00CA201603, R21EB025270, R01EB028143, R01HL165176, R01HL166522, R01CA282451), the National Science Foundation (CBET-EBMS-1936105, CISE-IIS-2225698), and the Brigham Research Institute.

## Appendix A. Supplementary data

Supplementary data to this article can be found online at https://doi.org/10.1016/j.mtbio.2025.101449.

## Data availability

Data will be made available on request.

## References

[1] E.C. Butcher, E.L. Berg, E.J. Kunkel, Systems biology in drug discovery, Nat. Biotechnol. 22 (2004) 1253–1259.
[2] J.K. Nicholson, E. Holmes, J.C. Lindon, I.D. Wilson, The challenges of modeling mammalian biocomplexity, Nat. Biotechnol. 22 (2004) 1268–1274.
[3] B.A. Ruggeri, F. Camp, S. Miknyoczki, Animal models of disease: pre-clinical animal models of cancer and their applications and utility in drug discovery, Biochem. Pharmacol. 87 (2014) 150–161.
[4] T. Denayer, T. Stöhr, M. Van Roy, Animal models in translational medicine: validation and prediction, New Horizons Transl. Med 2 (2014) 5–11.
[5] P. McGonigle, B. Ruggeri, Animal models of human disease: challenges in enabling translation, Biochem. Pharmacol. 87 (2014) 162–171.
[6] N. Shanks, R. Greek, J. Greek, Are animal models predictive for humans? Philos. Ethics Humanit. Med. 4 (2009) 2.
[7] I.W.Y. Mak, N. Evaniew, M. Ghert, Lost in translation: animal models and clinical trials in cancer treatment, Am. J. Transl. Res. 6 (2014) 114.
[8] M. Wadman, FDA no longer needs to require animal tests before human drug trials, Science 379 (2023) 127–128.
[9] V. Brancato, J.M. Oliveira, V.M. Correlo, R.L. Reis, S.C. Kundu, Could 3D models of cancer enhance drug screening? Biomaterials 232 (2020) 119744.
[10] P. Neužil, S. Giselbrecht, K. Länge, T.J. Huang, A. Manz, Revisiting lab-on-a-chip technology for drug discovery, Nat. Rev. Drug Discov. 11 (2012) 620–632.
[11] M. Ravi, V. Paramesh, S.R. Kaviya, E. Anuradha, F.D.P. Solomon, 3D cell culture systems: advantages and applications, J. Cell. Physiol. 230 (2015) 16–26.
[12] L. Neufeld, E. Yeini, S. Pozzi, R. Satchi-Fainaro, 3D bioprinted cancer models: from basic biology to drug development, Nat. Rev. Cancer 22 (2022) 679–692.
[13] E. Knight, S. Przyborski, Advances in 3D cell culture technologies enabling tissue-like structures to be created in vitro, J. Anat. 227 (2015) 746–756.
[14] Y. Li, K.A. Kilian, Bridging the gap: from 2D cell culture to 3D microengineered extracellular matrices, Adv. Healthc. Mater. 4 (2015) 2780–2796.
[15] L. Moroni, et al., Biofabrication strategies for 3D in vitro models and regenerative medicine, Nat. Rev. Mater. 3 (2018) 21–37.
[16] M.A. Heinrich, et al., 3D bioprinting: from benches to translational applications, Small 15 (2019) 1805510.
[17] Y.S. Zhang, et al., 3D bioprinting for tissue and organ fabrication, Ann. Biomed. Eng. 45 (2017) 148–163.
[18] R. Levato, et al., From shape to function: the next step in bioprinting, Adv. Mater. 32 (2020) 1906423.
[19] B.L. LeSavage, R.A. Suhar, N. Broguiere, M.P. Lutolf, S.C. Heilshorn, Next-generation cancer organoids, Nat. Mater. 21 (2022) 143–159.
[20] I.T. Ozbolat, W. Peng, V. Ozbolat, Application areas of 3D bioprinting, Drug Discov. Today 21 (2016) 1257–1271.
[21] Y.S. Zhang, et al., 3D extrusion bioprinting, Nat. Rev. Methods Prim. 1 (2021) 75.
[22] W. Li, et al., Photopolymerizable biomaterials and light-based 3D printing strategies for biomedical applications, Chem. Rev. 120 (2020) 10950–11027.
[23] S.V. Murphy, A. Atala, 3D bioprinting of tissues and organs, Nat. Biotechnol. 32 (2014) 773–785.
[24] R. Levato, et al., Light-based vat-polymerization bioprinting, Nat. Rev. Methods Prim. 3 (2023) 47.
[25] K.S. Lim, et al., Fundamentals and applications of photo-cross-linking in bioprinting, Chem. Rev. 120 (2020) 10662–10694.
[26] X. Kuang, et al., Grayscale digital light processing 3D printing for highly functionally graded materials, Sci. Adv. 5 (2024) eaav5790.
[27] Z. Zhao, X. Tian, X. Song, Engineering materials with light: recent progress in digital light processing based 3D printing, J. Mater. Chem. C 8 (2020) 13896–13917.
[28] H. Goodarzi Hosseinabadi, E. Dogan, A.K. Miri, L. Ionov, Digital light processing bioprinting advances for microtissue models, ACS Biomater. Sci. Eng. 8 (2022) 1381–1395.
[29] J. Zhang, Digital light processing based three-dimensional printing for medical applications, IJB 6 (2019) 242.
[30] I. Matai, G. Kaur, A. Seyedsalehi, A. McClinton, C.T. Laurencin, Progress in 3D bioprinting technology for tissue/organ regenerative engineering, Biomaterials 226 (2020) 119536.
[31] M.W. Dewhirst, T.W. Secomb, Transport of drugs from blood vessels to tumour tissue, Nat. Rev. Cancer 17 (2017) 738–750.
[32] G. Mbalaviele, et al., E-cadherin expression in human breast cancer cells suppresses the development of osteolytic bone metastases in an experimental metastasis Model1, Cancer Res. 56 (1996) 4063–4070.
[33] Ş. Comşa, A.M. Cîmpean, M. Raica, The story of MCF-7 breast cancer cell line: 40 years of experience in Research, Anticancer Res. 35 (2015) 3147–3154.
[34] B. Pasculli, R. Barbano, P. Parrella, Epigenetics of breast cancer: biology and clinical implication in the era of precision medicine, Semin. Cancer Biol. 51 (2018) 22–35.
[35] R. Yerushalmi, R. Woods, P.M. Ravdin, M.M. Hayes, K.A. Gelmon, Ki67 in breast cancer: prognostic and predictive potential, Lancet Oncol. 11 (2010) 174–183.
[36] J.L. Sebaugh, Guidelines for accurate EC50/IC50 estimation, Pharm. Stat. 10 (2011) 128–134.
[37] A. Gebeyehu, et al., Polysaccharide hydrogel based 3D printed tumor models for chemotherapeutic drug screening, Sci. Rep. 11 (2021) 372.
[38] T.J. Flanigan, J.E. Anderson, I. Elayan, A.R. Allen, S.A. Ferguson, Effects of cyclophosphamide and/or doxorubicin in a murine model of postchemotherapy cognitive impairment, Toxicol. Sci. 162 (2018) 462–474.
[39] A.N. Chivate, P.S. Salve, R.C. Doijad, A.M. Mane, N.D. Chivate, Acute toxicity study of intravenously administered capecitabine resealed erythrocytes in mice, Res. J. Pharm. Technol. 15 (2022) 5473–5477.
[40] S. Reagan-Shaw, M. Nihal, N. Ahmad, Dose translation from animal to human studies revisited, FASEB J. 22 (2008) 659–661.
[41] A.T. Feldman, D. Wolfe, in: C.E. Day (Ed.), Tissue Processing and Hematoxylin and Eosin Staining BT - Histopathology: Methods and Protocols, Springer, New York, 2014, pp. 31–43, https://doi.org/10.1007/978-1-4939-1050-2_3.
[42] J.G. Moffat, F. Vincent, J.A. Lee, J. Eder, M. Prunotto, Opportunities and challenges in phenotypic drug discovery: an industry perspective, Nat. Rev. Drug Discov. 16 (2017) 531–543.
[43] K.P. Mishra, L. Ganju, M. Sairam, P.K. Banerjee, R.C. Sawhney, A review of high throughput technology for the screening of natural products, Biomed. Pharmacother. 62 (2008) 94–98.
[44] J. Gong, et al., Digital light processing (DLP) in tissue engineering: from promise to reality, and perspectives, Biomed. Mater. 17 (2022) 62004.
[45] R.G. Gish, et al., Phase III randomized controlled trial comparing the survival of patients with unresectable hepatocellular carcinoma treated with nolatrexed or doxorubicin, J. Clin. Oncol. 25 (2007) 3069–3075.
[46] M.E.R. O'Brien, et al., Reduced cardiotoxicity and comparable efficacy in a phase IIItrial of pegylated liposomal doxorubicin HCl(CAELYX™/Doxil®) versus conventional doxorubicin forfirst-line treatment of metastatic breast cancer, Ann. Oncol. 15 (2004) 440–449.
[47] S. Todd, Xeloda dosage. https://www.medicalnewstoday.com/articles/drugs-xeloda-dosage, 2024.
[48] M.A. Theodoraki, et al., Spontaneously-forming spheroids as an in vitro cancer cell model for anticancer drug screening, Oncotarget 6 (25) (2015).
[49] V. Das, et al., Pathophysiologically relevant in vitro tumor models for drug screening, Drug Discov. Today 20 (2015) 848–855.
[50] V.E. Santo, et al., Drug screening in 3D in vitro tumor models: overcoming current pitfalls of efficacy read-outs, Biotechnol. J. 12 (2017) 1600505.